**Rare Metal Materials and Engineering**
Volume 48, Issue 2, February 2019
Available online at www.rmme.ac.cn

Science Press

**Cite this article as:** Rare Metal Materials and Engineering, 2019, 48(2): 0426-0432.

ARTICLE

# Preferred Formation and Crystallographic Analysis of Three-variant Cluster in Zr-Cr-Fe Alloy During Martensitic Transformation

**Wang Jianmin[1], Liang Yuyang[1], Qiu Risheng[1], Luan Baifeng[1], Murty K L[2], Liu Qing[1]**

*[1] Chongqing University, Chongqing 400044, China; [2] North Carolina State University, Raleigh 27695-7909, USA*

**Abstract:** The martensitic microstructure of Zr-Cr-Fe alloy after $\beta$-quenching was investigated by a combination of electron channeling contrast (ECC) imaging, transmission electron microscopy (TEM) and electron backscatter diffraction (EBSD) techniques. The results show that all of theoretical 12 $\alpha$ variants inherited from one single $\beta$ phase have been obtained that reveal strict Burgers orientation relationship (BOR) with respect to $\beta$ parent phase. The entire martensitic microstructure consisting of these 12 $\alpha$ variants in the as-quenched Zr-Cr-Fe alloy can be divided into four sub-regions. Each sub-region, in turn, is dominated by only one type of three-variant cluster (one crystallographic group composed of three $\alpha$ variants) showing the self-accommodation triangular morphologies. These three variants from individual cluster share a common $<111>_\beta$ pole of $\beta$ parent phase and are related to each other by an angle/axis pair $60^\circ / <11\bar{2}0>$. The preferred formation of such three-variant cluster is ascribed to the elastic interaction between variants to achieve the largest degree of self-accommodation.

**Key words:** Zr-Cr-Fe alloy; Burgers orientation relationship; self-accommodation; three-variant cluster

Zr alloys are widely used as fuel cladding tubes in nuclear water reactors by virtue of their sufficient mechanical strength, excellent corrosion resistance, and particularly, low thermal neutron absorption cross section[1-3]. For conventional fabrication technologies in Zr alloys, $\beta$-quenching is mainly employed to tailor microstructure prior to subsequent thermo-mechanical treatments. During such process, martensitic transformation between $\beta$ parent phase (bcc) and $\alpha$ product phase (hcp) in Zr alloys is usually activated. Theoretically, the $\alpha$ product phase generally follows the well-known Burgers orientation relationship with respect to $\beta$ parent phase, i.e., $\{110\}_\beta||\{0001\}_\alpha$ and $<111>_\beta||<11\bar{2}0>_\alpha$[4]. Based on Burgers orientation relationship (BOR) and the symmetries of the cubic ($\beta$ parent phase) and hexagonal structures ($\alpha$ product phase), one single $\beta$ parent phase can transform into 12 $\alpha$ product phases with distinct orientations, which are referred to be variants listed in Table 1[5]. When two different $\alpha$ variants adjoin in one prior $\beta$ grain, a special intervariant boundary is usually formed. Due to the crystal symmetry, all possible intervariant boundaries formed in the system can be described by only five independent misorientation angles and axis pairs, as tabulated in Table 2[6].

With respect to the martensitic transformation, one important aspect is that the nucleation and growth of product phase would lead to significant shape strains of the surrounding parent matrix. Therefore, the system will favor the reduction of the overall strain energy through the so-called self-accommodation[7-9]. Accordingly, different types of clusters consisting of two or three variants showing various self-accommodation morphologies would be formed in different alloy systems. For instance, three-variant cluster showing triangular self-accommodation morphology has been observed in CuAlNi[10], pure Ti[11] and Ti-Nb-Al[12] alloys. In the meantime, two- variant cluster exhibiting V-shaped morphology in Ti-Nb[13] and $\beta$-Ti[14] and four-variant cluster having diamond-shaped morphology in Ag-Cd alloys[15] and $Co_{50}Ni_{20}Ga_{30}$[16] were also reported.

Received date: February 21, 2018
Foundation item: National Natural Science Foundation of China (51371202, 51531005, 51421001, 51501021); Fundamental Research Funds for the Central Universities (106112017CDJQJ138803)
Corresponding author: Luan Baifeng, Professor, College of Materials Science and Engineering, Chongqing University, Chongqing 400044, P. R. China, Tel: 0086-23-65106067, E-mail: bfluan@cqu.edu.cn

**Table 1 Twelve possible variants generated by the $\beta \rightarrow \alpha$ martensitic phase transformation through the Burgers orientation relationship[5]**

| Variant No. | Plane parallel | Direction parallel |
|---|---|---|
| V1 | $(1\bar{1}0)_\beta \parallel (0001)_\alpha$ | $[111]_\beta \parallel [11\bar{2}0]_\alpha$ |
| V2 | $(10\bar{1})_\beta \parallel (0001)_\alpha$ | $[111]_\beta \parallel [11\bar{2}0]_\alpha$ |
| V3 | $(01\bar{1})_\beta \parallel (0001)_\alpha$ | $[111]_\beta \parallel [11\bar{2}0]_\alpha$ |
| V4 | $(110)_\beta \parallel (0001)_\alpha$ | $[\bar{1}11]_\beta \parallel [11\bar{2}0]_\alpha$ |
| V5 | $(101)_\beta \parallel (0001)_\alpha$ | $[\bar{1}11]_\beta \parallel [11\bar{2}0]_\alpha$ |
| V6 | $(01\bar{1})_\beta \parallel (0001)_\alpha$ | $[\bar{1}11]_\beta \parallel [11\bar{2}0]_\alpha$ |
| V7 | $(110)_\beta \parallel (0001)_\alpha$ | $[1\bar{1}1]_\beta \parallel [11\bar{2}0]_\alpha$ |
| V8 | $(10\bar{1})_\beta \parallel (0001)_\alpha$ | $[1\bar{1}1]_\beta \parallel [11\bar{2}0]_\alpha$ |
| V9 | $(011)_\beta \parallel (0001)_\alpha$ | $[1\bar{1}1]_\beta \parallel [11\bar{2}0]_\alpha$ |
| V10 | $(1\bar{1}0)_\beta \parallel (0001)_\alpha$ | $[11\bar{1}]_\beta \parallel [11\bar{2}0]_\alpha$ |
| V11 | $(101)_\beta \parallel (0001)_\alpha$ | $[11\bar{1}]_\beta \parallel [11\bar{2}0]_\alpha$ |
| V12 | $(011)_\beta \parallel (0001)_\alpha$ | $[11\bar{1}]_\beta \parallel [11\bar{2}0]_\alpha$ |

**Table 2 Specific angle/axis pair between $\alpha$ variants inherited from the same $\beta$ grain according to Burgers relationship[6]**

| Type | Axis/angle pairs | Frequency/% |
|---|---|---|
| 1 | $10.5°/[0001]$ | 9.2 |
| 2 | $60°/[11\bar{2}0]$ | 18.2 |
| 3 | $60.8°/[11\bar{2}3]$ | 36.4 |
| 4 | $63.3°/[44\bar{8}3]$ | 18.2 |
| 5 | $90°/[12\bar{3}0]$ | 18.2 |

Besides to the experimental studies, extensive theoretical calculations have also been carried out to explore the formation mechanism of different types of variant clusters during martensitic transformation. Meng et al[17] have calculated average shape deformation of different combinations of variants in the Ti-Ni-Cu thin film based on classical phenomenological theory of martensite crystallography (PTMC). It is shown that for triangular self-accommodation morphology, the diagonal elements of the average shape deformation approach unity and the off-diagonal terms approach zero, suggesting that the total shape change is minimized. For single pair morphology, the average shape deformation is larger than that for triangular self-accommodation morphology, indicating that the single pair morphology of martensite cannot release the transformation strain efficiently in one grain. Applying a similar method, Wang et al[11] have calculated the individual shape strain of the 12 variants originated from the martensitic transformation as well as the average shape strain of three-variant cluster and four- variant cluster in pure titanium. It is concluded that the three- variant cluster would give the greatest degree of self-accommodation. More recently, Balachandran et al[18] have investigated the stereology and distribution of $\alpha$ variant generated from the $\beta$ (bcc) matrix in Ti5553 alloy by calculating the effective Von-Mises strain to analyze the elastic interaction between different pairs of variants. It is established that the interaction energies between variants reach minimum when 3 variants cluster into one group in which these variants are related to each other by an angle-axis pair $60°/<11\bar{2}0>$. In addition, Chai et al[13] have investigated the self-accommodation behavior of the $\alpha$" martensites in Ti-Nb shape memory alloys with Nb content ranging from 20 at% to 24 at%. It has been reported that the different viewed-orientation or a different level of sectioning through the tetrahedron would also result in different self-accommodation morphologies.

In spite of these previous extensive studies on various alloys, the formation of variant cluster in Zr alloys during martensitic transformation, especially in the case of a recently developed Zr-Cr-Fe alloy systems[19] has not been fully understood. Therefore, the principal focuses of the present paper are as follows:

(i) To characterize the morphologies of distinct orientation $\alpha$ variants arranged in Zr-Cr-Fe alloy and clarify the crystallographic relationship between adjacent different $\alpha$ variants and between $\alpha$ variants and $\beta$ parent grain.

(ii) To explore the preferred formation mechanism of such three-variant cluster in the studied Zr-Cr-Fe alloy on the basis of the self-accommodation theory.

## 1 Experiment

The ternary Zr alloy with nominal composition of Zr-1.0Cr-0.4Fe (wt%) was prepared from nuclear grade sponge Zr and high-purity Cr and Fe (99.99%) by a non-consumable arc-melting method. This alloy was remelted six times in order to obtain good homogeneity. Samples with dimensions of 10 mm×10 mm×2 mm were cut from the center part of the ingot and then heat treated at 1050 °C for 30 min followed by quenching in liquid nitrogen. The samples were sealed in evacuated quartz capsules under vacuum prior to any heat treatment to avoid oxidation.

The microstructures of the samples were characterized by ECC and EBSD technique. They were equipped within a FEI Nova 400 field emission gun scanning electron microscope. Prior to these examinations, the samples were mechanically ground and electrolytically polished in a solution of $CH_3OH:C_6H_{14}O_2:HClO_4$=7:2:1 at 20 V and −30 °C. The experimental samples characterized by transmission electron microscopy (TEM) were disks about 3 mm in diameter and about 0.05 mm in thickness. These disks were twin-jet polished in a solution of 10 vol% $HClO_4$ and 90 vol% $C_2H_5OH$ with a DC voltage of 30 V and a current of 20 mA at −40 °C. TEM observations were carried out using FEI Tecnai $G^2$ F20 operating at 200 kV.

## 2 Results and Discussion

### 2.1 Self-accommodation morphology of martensitic variants

Fig.1 presents the ECC images of $\beta$-quenched microstructure of Zr-Cr-Fe alloy. From the ECC map in Fig.1a, it appears that the prior $\beta$ grains are identifiable due to the reservation of prior $\beta$ grains boundaries (marked by white arrow) at room temperature, and the prior $\beta$ grain sizes vary from a few hundred micrometers to more than one millimeter. A typical region A in Fig.1a is further magnified in Fig.1b, from which we can see that the transformed microstructure is dominated by martensitic variants in interlaced form. These martensitic variants exhibit different contrasts in the ECC images due to distinct crystallographic orientations. Comparing the martensitic microstructure in the studied Zr-Cr-Fe alloy with that in other Zr alloy systems[20,21], one noticeable feature is that the entire martensitic structure is divided into many sub-regions (as indicated by black arrow in Fig.1b) showing different contrasts due to distinct crystallographic orientations. The finer morphology and substructure of such a representative sub-region B in Fig.1b are revealed by closer observation in Fig.1c. It can be seen that various $\alpha$ martensitic variants tend to distribute in a typical triangular morphology (as indicated by the dashed triangle in Fig.1c) within the sub-region. This triangular morphology can be further supported by bright-field TEM micrographs of $\beta$-quenched microstructure in Zr-Cr-Fe alloy, as shown in Fig.2. From Fig.2a, it is readily seen that various triangular morphologies have been obtained from the Zr-Cr-Fe alloy. A representative triangular morphology is further magnified in Fig.2b. It can be seen that this triangular morphology consists of three martensitic variants, marked as V1, V2 and V3. The crystallography and formation mechanisms of such three-variant cluster will be discussed extensively in the following sections.

### 2.2 Crystallography of the martensitic variants

In order to further clarify crystallographic characteristics of martensitic transformation in Zr-Cr-Fe alloy, an EBSD examination has been performed for the $\beta$-quenched microstructure.

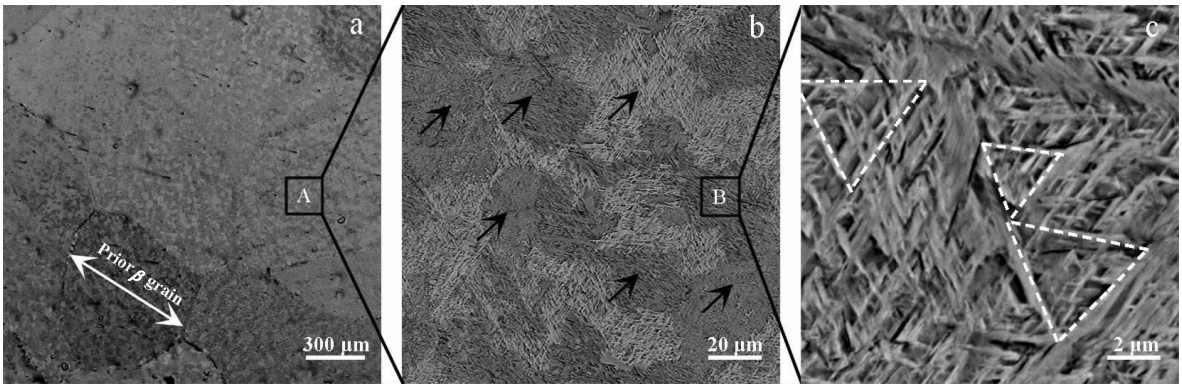


Fig.1 ECC images of the $\beta$-quenched microstructure in Zr-Cr-Fe alloy: (a) macroscopic microstructure, (b) magnified image of region A, and (c) magnified image region B

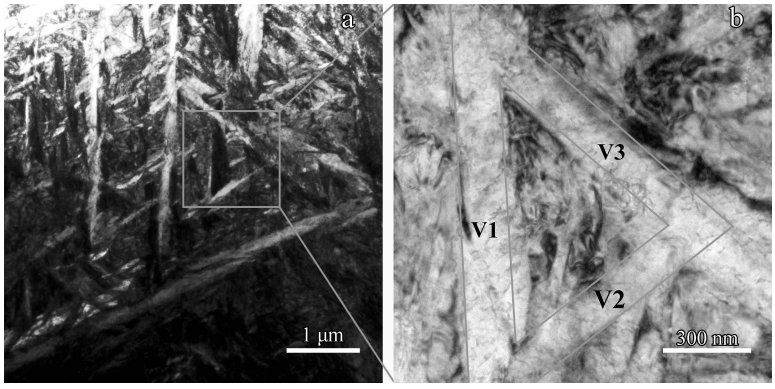


Fig.2 TEM bright-field micrographs of the microstructure of $\beta$-quenched Zr-Cr-Fe alloy (a) and the magnified image of the boxed region in Fig.2a showing triangular morphology of an aggregation of three variants (b)

Fig.3a shows an orientation imaging microscopy (OIM) of a typical lath martensite, where the entire area is divided into four distinct types of sub-regions (as indicated by white boxes 1~4). Crystallographic characteristics during martensitic transformation are described in term of {0001} and $<11\bar{2}0>$ pole figures, as shown in Fig.3b and 3c, respectively. It can be seen from these pole figures that all theoretical 12 $\alpha$ variants inherited from one single $\beta$ parent phase have been acquired in the present work, which are marked by consecutive numbers in Fig.3b and 3c. According to the {0001} pole figure, all of the 12 $\alpha$ variants are separated into six pairs. Each pair of variants, such as variants 1 and 2, makes their basal planes parallel with each other and share the common {110} plane of $\beta$ parent phase. In the case of $<11\bar{2}0>$ pole figure, however, these 12 $\alpha$ variants can be classified into four types of three-variant cluster (marked by circle in Fig.3c), in which each cluster is corresponding to one of four <111> directions of $\beta$ parent phase. The above results are completely consistent with the prediction according to the Burgers orientation relationship as shown in Table 1.

The misorientation angle distribution of martensite is further computed and presented in Fig.4, where three distinct peaks appear in angular ranges of 10°, 60° and 90°. It should be noted that the peak around 60° is actually formed by the superposition of three peaks close to angular ranges of 60°, 60.8° and 63.3°. They cannot be distinguished under the limited angular resolution of the EBSD technique due to these three peaks getting too close. Rotation axes of those measured misorientation angles are also analyzed and presented in Fig.4. The peak close to the angle range of 10° is associated with the rotation axes $[0001]$, as marked by I. The greatest peak around angle range of 60° reveals three distinct axes close to the rotation axes $[11\bar{2}0]$ (marked by II), $[123\bar{1}]$ (marked by III) and $[44\bar{8}3]$ (marked by IV). The peaks at the angle range of 90° correspond with the rotation axes of $[12\bar{3}0]$ (marked by V). These angle-axis pairs are quite similar to the theoretical predictions in Table 2. Therefore, the all above facts strongly suggest that the resulting $\alpha$ lath martensite in the Zr-Cr-Fe alloy obeys the typical Burgers orientation relationship with respect to $\beta$ parent phase.

### 2.3 Crystallographic analysis of the three-variant clusters

As mentioned in section 2.2, there are four types of sub-regions in total that dominate the entire detected region, as highlighted by boxes 1~4 in Fig.3a. To examine the crystallographic relationship between different variants within individual sub-region for more depth, all of the four sub-regions of interest are selected to enlarge in Fig.5. It is seen that the variants 1, 4 and 11 in Fig.5a and variants 2, 6 and 8 in Fig. 5c constitute sub-region 1 and sub-region 2, respectively. It is the same case for the sub-regions 3 in Fig.5e and sub-regions 4 in Fig.5g. This suggests that each of the four sub-regions is corresponding to one type of three-variant cluster. In fact, the occurrence of such three-variant cluster in specimens could be ascribed to the effect of self-accommodation that will be discussed in section 3 below. More orientation relationships between these different variants from individual three-variant cluster are revealed by {0001} and $<11\bar{2}0>$ pole figures in Fig.5b, 5d, 5f and 5h. Take the three-variant cluster in sub-

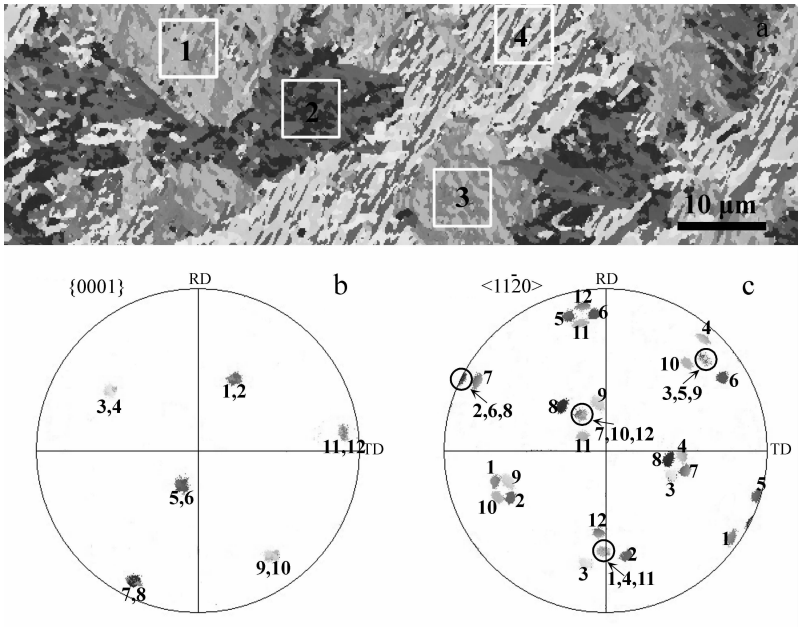


Fig.3 EBSD orientation imaging microscopy of a typical lath martensitic region in Zr-Cr-Fe alloy: (a) boxed areas are examples of four sub-regions; (b) {0001} and (c) <11$\bar{2}$0> pole figures of corresponding to region in Fig.3a; consecutive numbers represent various crystallographic orientations of 12 $\alpha$ variants transformed from the same $\beta$ grains

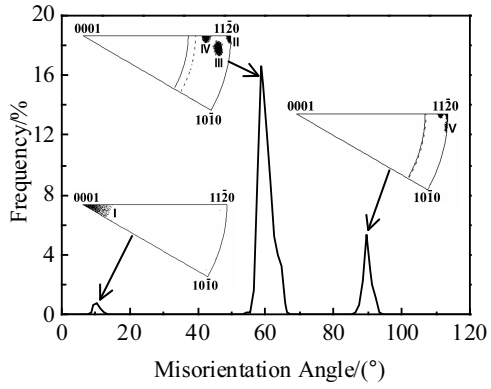


Fig.4 Misorientation angle histogram and rotation axis distribution corresponding to Fig.3a

region 1 as an example, in-depth analysis of $<11\bar{2}0>$ pole figure indicates that such three-variant cluster has a common axis $<11\bar{2}0>$ and is parallel to one of $<111>$ pole of the $\beta$ parent phase (marked by the open circle in $<11\bar{2}0>$ pole figure in Fig.5b). In addition, it is also clear that these three variants are about 60° between their *c* axes, as revealed by {0001} pole figures in Fig.5b. This holds the same rule for the other three types of sub-regions 2, 3 and 4. Accordingly, this orientation relationship between these three variants from each type of three-variant cluster can be expressed as angle/axis pair $60°/<11\bar{2}0>$. The above crystallography can be better visualized from the three-dimensional (3-D) crystal orientations associated with four sets of three-variant cluster as shown in Fig.5a, 5c, 5e and 5g.

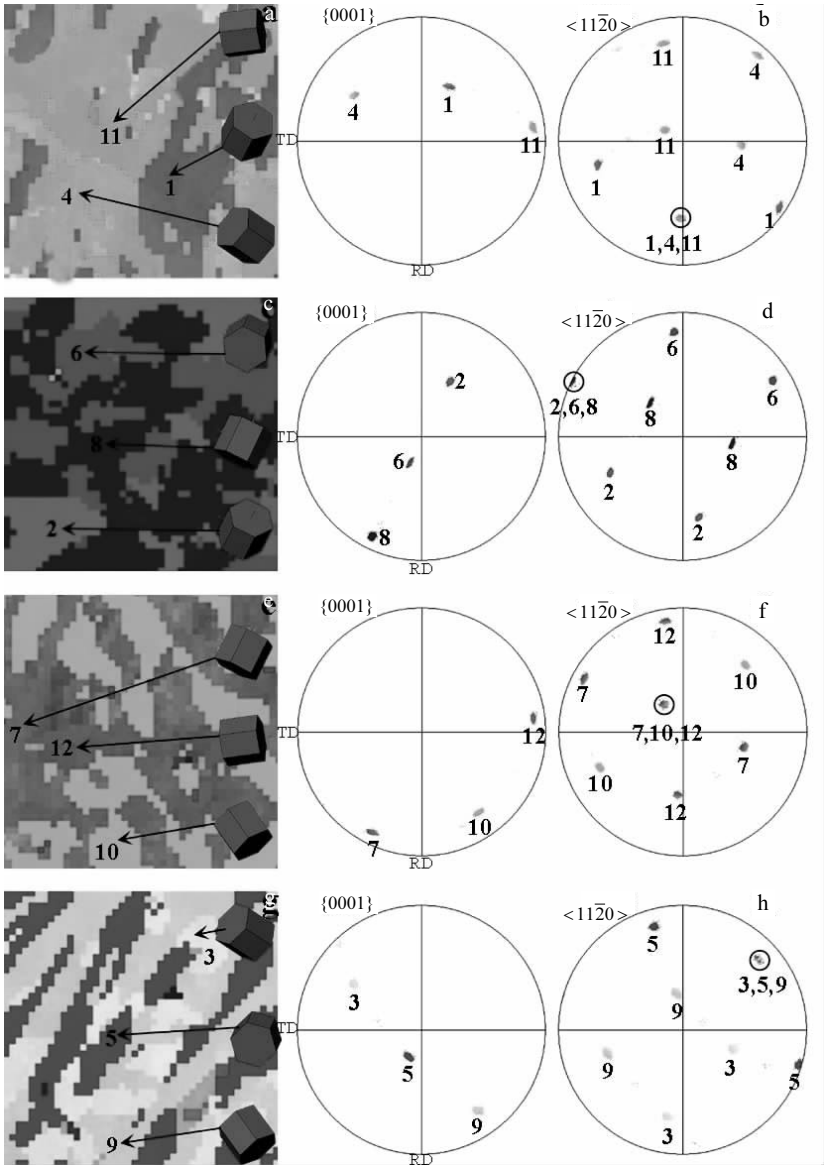


Fig.5 Enlarged images of the boxed regions 1~4 in Fig.3a (a, c, e, g) and the corresponding pole figures (b, d, f, h)

## 3 Discussions

In the current work, all possible 12 $\alpha$ variants inherited from one single $\beta$ parent phase have been acquired. These 12 $\alpha$ variants arrange themselves as typical triangular self-accommodation morphology. This triangular morphology is composed of three $\alpha$ variants cluster (V1, V2 and V3), as shown in Fig.2b. According to previous investigations, it seems that the distinct self-accommodation morphologies of martensitic variants formed in various alloys are closely related to the number of variants that aggregate into one cluster. It has been accepted in general that the three-variant cluster tends to arrange themselves as triangular self-accommodation morphology, while the two-variant and four-variant cluster would display themselves as V-shaped morphology and diamond-shaped morphology, respectively. For example, it has been reported by Chai et al[13] that the occurrence of three-$\alpha$" variant cluster in the Ti-Nb alloys during $\beta$-$\alpha$" martensitic transformation shows an typical triangular morphology, which clustered around the $<111>$ poles of parent phase. In addition to three-variant cluster, a two-$\alpha$" variants cluster showing V-shaped morphology was found to be another type of self-accommodation morphology in that study. Similarly, Inamura et al[14] have also found that three-variant cluster showing triangular self-accommodation morphology and two-variant cluster displaying V-shaped morphology coexist within a $\beta$-titanium shape memory alloy. As the case of cluster consisting of four variants, an extensive investigation has been performed by Saburi et al.[22]. It is found that this four-variant cluster sharing one of $<011>$ poles of the parent phase would develop into diamond-shaped self-accommodation morphology in Cu-Al-Zn shape memory alloy. Based on above rule, it seems reasonable to conclude that it is such aggregation of three $\alpha$ variants that results in the formation of typical triangular self-accommodation morphology in the studied Zr-Cr-Fe alloy.

Furthermore, we have established that all of these 12 $\alpha$ variants inherited from one prior $\beta$ parent grain tend to be divided into four types of three-variant cluster in this case. These three variants aggregate around one of $<111>$ poles of parent phase and are related to each other by an angle/axis pair $60^{o}/<11\bar{2}0>$. Each type of three-variant cluster is actually corresponding to one type of sub-regions, as shown in Fig.3a. Theoretically, the preferred formation of these three-variant clusters in Zr-Cr-Fe alloy during martensitic transformation is ascribed to the elastic interaction between variants to achieve the largest degree of self-accommodation. With respect to Zr alloys, the degrees of self-accommodation for distinct variant clusters have been computed based on classical phenomenological theory of martensite crystallography[23]. It is clearly shown that, among all cases considered, the degree of self-accommodation would reach maximum (91.28%) when 3 variants cluster into one group around $<111>$ poles of parent phase. Therefore, it seems very reasonable for the three-variant cluster preferring in Zr-Cr-Fe alloys during martensitic transformation from the point of self-accommodation effect. The effect of self-accommodation on microstructure of other various alloys during martensitic transformation has also been investigated. For example, a similar triangular morphology consisting of three variants is also found to be formed in Ti-Ni alloys during martensitic transformation in which these three variants are related to each other around one of {100} poles[24]. The calculated shape strain matrix for the overall triangular morphology shows that the shear components of the shape strain, although non-zero, are numerically quite small. This means that the mechanical driving force tends to prefer the formation of three-variant cluster in this system. This self accommodation effect has also been reported in bainitic microstructure of ultra-high-strength steel, where the shape strain is minimized by the formation of four distinct sheaf colonies of bainite variants arrangements. Each sheaf colony, in turn, is made of one crystallographic group composed of three variants of bainite, and one from each of the three Bain correspondences[25].

## 4 Conclusions

1) All of theoretical 12 $\alpha$ variants have been detected in one prior $\beta$ grain that reveals strict Burgers orientation relationship with respect to $\beta$ parent phase.

2) Four types of three-variant cluster have separated the entire martensitic microstructure into four sub-regions. These three variants from each cluster share one of $<111>_{\beta}$ pole of parent phase and are related to each other by an angle/axis pair $60^{o}/<11\bar{2}0>$.

3) Each type of three-variant cluster shows the self-accommodation triangular morphologies. The preferred formation of such three-variant cluster is ascribed to the elastic interaction between variants to achieve the largest degree of self-accommodation.

## References


1 Bai G H, Wang R S, Zhang Y W *et al*. *Rare Metal Materials and Engineering*[J], 2016, 45(10): 2473

2 Chai L J, Luan B F, Murty K L *et al*. *Acta Materialia*[J], 2013, 61(8): 3099

3 Liu Y Z, Hyun G K, Jeong Y P *et al*. *Rare Metal Materials and Engineering*[J], 2013, 42(4): 667

4 Burgers W G. *Physica*[J], 1934, 1(7): 561

5 Beladi H, Qi C, Rohrer G S. *Acta Materialia*[J], 2014, 80: 478

6 Chai L J, Luan B F, Zhang M *et al*. *Journal of Nuclear Materials*[J], 2013, 440(1-3): 377

7 Chulist R, Böhm A, Oertel C G *et al*. *Journal of Materials Science*[J], 2014, 49(11): 3951

8 Waitz T. *Acta Materialia*[J], 2005, 53(8): 2273

9 Chulist R, Faryna M, Szczerba M J. *Journal of Materials Science*[J], 2016, 51(24): 10 943

10 Sarï U, ilhan A. *Journal of Materials Processing Technology*[J], 2008, 195(1-3): 72
11 Wang S C, Aindow M, Starink M J. *Acta Materialia*[J], 2003, 51(9): 2485
12 Inamura T, Hosoda H, Kanetaka H *et al*. *Mater Sci Forum*[J], 2010, 654-656: 2154
13 Chai Y W, Kim H Y, Hosoda H *et al*. *Acta Materialia*[J], 2009, 57(14): 4054
14 Inamura T, Hosoda H, Miyazaki S. *Philosophical Magazine A*[J], 2013, 93(6): 618
15 Saburi T, Wayman C M. *Acta Metallurgica*[J], 1980, 28(1): 15
16 Meng F B, Li Y X, Liu H Y *et al*. *Journal of Materials Science and Technology*[J], 2004, 20(6): 697
17 Meng X L, Sato M, Ishida A. *Scripta Materialia*[J], 2008, 59(4): 451
18 Balachandran S, Kashiwar A, Choudhury A *et al*. *Acta Materialia*[J], 2016, 106: 374
19 Wei T, Long C, Luan B *et al*. *Rare Metal Materials and Engineering*[J], 2013, 42(12): 2553 (in Chinese)
20 Chai L J, Chen B F, Zhou Z M *et al*. *Materials Characterization*[J], 2015, 104: 61
21 Yang H Y, Kano S, Matsukawa Y *et al*. *Materials Design*[J], 2016, 104: 355
22 Saburi T, Wayman C M. *Acta Metallurgica*[J], 1979, 27(6): 979
23 Srivastava D, Madangopal K, Banerjee S *et al. Acta Metallurgica et Materialia*[J], 1993, 41(12): 3445
24 Miyazaki S, Otsuka K, Wayman C M. *Acta Metallurgica*[J], 1989, 37(7): 1873
25 Pancholi V, Krishnan M, Samajdar L S *et al*. *Acta Materialia*[J], 2008, 56(9): 2037

# Zr-Cr-Fe 合金马氏体相变过程中三变体团簇的择优形成及其晶体学分析

王建民[1]，梁御阳[1]，邱日盛[1]，栾佰峰[1]，Murty K L[2]，刘 庆[1]

(1. 重庆大学，重庆 400044)

(2. 北卡罗莱纳州立大学，罗利 27695-7909，美国)

**摘 要**：采用 ECC, TEM 和 EBSD 表征技术，研究了 Zr-Cr-Fe 合金经 $\beta$ 相淬火后的马氏体组织特征。结果表明：马氏体相变过程中，任一高温 $\beta$ 相都能够转变为 12 个 $\alpha$ 马氏体变体。而这 12 个 $\alpha$ 马氏体变体并不是随机分布的，而是择优形成了 4 个亚区域。每一个亚区域由一种三变体团簇组成，而该三变体团簇表现为典型的三角形自我协调形貌。进一步晶体学分析表明：组成每一个团簇的这 3 个马氏体变体与母相之间存在一个共同的 $<111>_{\beta}$ 极点，同时该三变体相互之间的取向关系为 $60^{\circ}/<11\bar{2}0>$。由于在 $\beta\rightarrow\alpha$ 马氏体相变过程中存在形状应变，而三变体团簇的形成能够最大程度的协调该应变。

**关键词**：Zr-Cr-Fe；Burgers 取向关系；自我协调；三变体团簇

作者简介：王建民，男，1988 年生，博士，重庆大学材料科学与工程学院，重庆 400044，电话：023-65106067，E-mail: 543696146@qq.com